M. A. Farrokhzad* and T. I. Khan

High Temperature Oxidation of Nickel-based Cermet Coatings Composed of Al_2O_3 and TiO_2 Nanosized Particles

Abstract: New technological challenges in oil production require materials that can resist high temperature oxidation. In-Situ Combustion (ISC) oil production technique is a new method that uses injection of air and ignition techniques to reduce the viscosity of bitumen in a reservoir and as a result crude bitumen can be produced and extracted from the reservoir. During the in-situ combustion process, production pipes and other mechanical components can be exposed to air-like gaseous environments at extreme temperatures as high as 700 °C. To protect or reduce the surface degradation of pipes and mechanical components used in in-situ combustion, the use of nickel-based ceramic-metallic (cermet) coating produced by co-electrodeposition of nanosized Al_2O_3 and TiO_2 have been suggested and earlier research on these coatings have shown promising oxidation resistance against atmospheric oxygen and combustion gases at elevated temperatures. Co-electrodeposition of nickel-based cermet coatings is a low-cost method that has the benefit of allowing both internal and external surfaces of pipes and components to be coated during a single electroplating process. Research has shown that the volume fraction of dispersed nanosized Al_2O_3 and TiO_2 particles in the nickel matrix which affects the oxidation resistance of the coating can be controlled by the concentration of these particles in the electrolyte solution, as well as the applied current density during electrodeposition. This paper investigates the high temperature oxidation behaviour of novel nanostructured cermet coatings composed of two types of dispersed nanosized ceramic particles (Al_2O_3 and TiO_2) in a nickel matrix and produced by co-electrodeposition technique as a function of the concentration of these particles in the electrolyte solution and applied current density. For this purpose, high temperature oxidation tests were conducted in dry air for 96 hours at 700 °C to obtain mass changes (per unit of area) at specific time intervals. Statistical techniques as described in ASTM G16 were used to formulate the oxidation mass change as a function of time. The cross-section and surface of the oxidized coatings were examined for both visual and chemical analyses using wavelength dispersive x-ray spectroscopy (WDS) element mapping, X-ray Diffraction (XRD) and Energy-dispersive X-ray spectroscopy (EDS). The results showed that the volume fraction for each type of particle in the nickel matrix corresponded to its partial molar concentration in the electrolyte solutions. Increase in volume fraction of particles in the nickel matrix was correlated to lower oxidation rates. It was concluded that formation of Ni_3TiO_5 and $NiTiO_3$ compounds can reduce the oxidation rate of cermet coatings by capturing some inward diffusing oxygen ions resulting in a lower number of nickel cations diffusing upward into the oxide layer.

Keywords: co-electrodeposition, current density, nanostructured cermet coatings, high temperature oxidation, $NiTiO_3$, Ni_3TiO_5

PACS® (2010). 68, 81, 82

***Corresponding author: M. A. Farrokhzad:** Department of Mechanical and Manufacturing Engineering, University of Calgary, Canada. E-mail: mafarrok@gmail.com
T. I. Khan: Department of Mechanical and Manufacturing Engineering, University of Calgary, Canada

1 Introduction

In recent years, the quest for oil has taken some technological approaches to use extreme conditions to produce oil from unconventional oil reservoirs such as the tar-sands of Alberta. One of these techniques is know as in-situ combustion, which utilizes injecting air and ignition techniques to burn the un-extractable light hydrocarbon grades. As a result of heat produced during the combustion process, the viscosity of heavier hydrocarbon grades will be reduced and therefore, they can be extracted easier. During the combustion process, the production pipe and mechanical components can be exposed to oxidizing air at temperatures as high as 700 °C [1]. These conditions are detrimental to all metals and alloys and eventually designed pressure thickness of the components and pipe can be harmed as a result of oxidation. Therefore, it is essential to protect the surface of the pipe and mechanical

components by oxidation resistance coatings that can cause a delay or reduce the rapidness of the oxidation process and therefore, extend the life of components. Co-electrodeposition of cermet coatings composed of nanosized Al_2O_3 and TiO_2 particles dispersed in a nickel matrix (as novel materials) have been suggested to be used for in-situ combustion applications and some earlier research on oxidation of these materials have shown promising results in delaying the oxidation progression into the bulk of the material. Research has shown that the volume fractions of dispersed nanosized Al_2O_3 and TiO_2 particles in the nickel matrix (which affects the oxidation resistance of the coating) can be controlled by the concentration of these particles in the electrolyte solutions and as well as the applied current density during electrodeposition. This paper investigates the high temperature oxidation behaviour of novel nanostructured cermet coatings composed of two types of dispersed nanosized ceramic particles (Al_2O_3 and TiO_2) in a nickel matrix and produced by co-electrodeposition technique as a function of concentration of these particles in the electrolyte solution and applied current density.

In general the electrocrystallization process of making cermet materials can be divided into two individual electrochemical reactions: 1) electrodeposition of matrix metal on the substrate, 2) attraction and trapping of electrically inert ceramic particles into the deposited matrix governed by electrophoresis phenomenon. Electrodeposition (or electrocrystallization) of metals is a mass transfer process from the anode to the cathode through the electrolyte solution during the electrolysis process where the anode dissolves into charged metal cations in the electrolyte solution ($M_0 - e^- \rightarrow M^+$). Simultaneously these cations migrate toward the cathode and then are deposited on the cathode surface (substrate) by receiving electrons from applied current ($M^+ + e^- \rightarrow M_0$) to complete the electric circuit. In the electrodeposition technique, the following steps may occur during the mass transfer (or cathodic discharge) process [2]:

1. Migration of ions to the cathode and through the electrode double layer (Helmholtz plane) to the surface in which hydration molecules are lost;
2. Ion adsorption on the metal surface as an "adion";
3. Adion diffusion on the metal surface to the discharge site of the minimum surface energy;
4. Ionic discharge and electron transfer.

Faraday's laws of electrolysis can be applied for measuring the deposition of material during electrodeposition. Faraday's first law states that the weight gain W during electrodeposition (mass transfer through electrolysis) is proportional to the current i and time t and electrochemical equivalent Z:

$$W = Zit \tag{1}$$

Faraday's second law states that for a given quantity of electric charge, the weight (mass) of an element discharged is proportional to the element's equivalent weight.

$$W = \frac{itA}{nF} \tag{2}$$

where A is the atomic weight, F is Faraday's constant and n is the number of electrons transferred. Unlike the electrodeposition of metals, in electrophoresis deposition no electron is exchanged and the migration of electrically inert particles is of an electrostatic attraction nature. These relatively large oxide particles are electrostatically charged as a result of interaction of their ionic and dipolar characteristics with the applied electric potential field between the anode and cathode across the electrolyte. The electrostatic charge potential corresponds to the difference in potential between the particle and the stationary fluid layer (or electrical double layer) from the electrolyte solution (surrounding the particles) and is known as zeta potential (ζ). The amount of zeta potential can be calculated as [2]:

$$\zeta = \frac{4\pi ed}{D} \tag{3}$$

where e is the electric charge per unit of area, d is the spacing of the parallel plates of the double layer, and D is the dielectric constant. The electric field E exerts a force (also known as electric force or F_E) on the electrostatically charged particles, which is equal to $F_E = Exe$. If the exerted electric force is greater or equal to the frictional drag resistance force from the liquid electrolyte (F_D), then the particles start migrating towards the cathode. The amount of the drag resistance force is equal to [2]:

$$F_D = \frac{\eta \times u}{d} \tag{4}$$

Therefore:

$$E \times e = \frac{\eta \times u}{d} \quad \text{or we can have:} \quad d = \frac{\eta \times u}{E \times e} \tag{5}$$

where η is the coefficient of velocity, u is the uniform velocity of moving particles. And by substituting d in the zeta potential equation, for a steady state condition:

$$\zeta = \frac{4\pi\eta \times u}{DE} \tag{6}$$

Recent research on oxidation behaviour of nickel-based cermet coatings has shown that compared to the pure form of metals and alloys, these cermet coatings can have better oxidation resistances in air-like gaseous environments at elevated temperatures [3, 4]. To quantify the oxidation behaviour metals, several theories have been developed in the past. One of these theories was developed by Carl Wagner in the 1930s and utilizes and reformulates Fick's diffusion laws based on the exchange rate of inward diffusion ions from gas and upward diffusion of cations from metal through the growing oxide layer. Wagner's theory provides a parabolic rate equation in which the oxide film growth rate for pure metals is controlled by diffusion of charged particles, such as electrons, cations and ions, across the oxide layer [5–8]. The Wagner's solution to the diffusion equation for oxidation of metals which defines the growth rate of the oxide layer can be simplified to [9]:

$$\left(\frac{\Delta m}{A}\right)^2 = k't \tag{7}$$

where k' is the parabolic rate of oxidation constant when measuring mass change per unit of area during the oxidation. The research on high temperature oxidation of electrodeposited composite coating by Susan and Marder has shown that the oxidation rates for these coatings can be better described by a modified version of Wagner's solution [10, 11]:

$$\frac{\Delta m}{A} = kt^a + C \tag{8}$$

where k is called the oxidation rate constant, a is called the growth time constant and C is a general constant of integration. Nickel-based cermet coatings composed of Al_2O_3 have much greater hardness compared to pure nickel coatings and therefore they are used as a protective layer against wear and erosion [12–15]. Additionally, cermet coatings composed of nanosized TiO_2 incorporated in a nickel matrix have shown improved thermal stability against high temperature oxidation [16]. Until now, there has been no study on the oxidation performance of nickel-based cermet coatings when both Al_2O_3 and TiO_2 particles are incorporated in the matrix. Based on our initial research conducted on cermet coatings composed of only one type of Al_2O_3 or TiO_2 particles, it is believed that nickel-based cermet coatings with both TiO_2 and Al_2O_3 can potentially have the benefits of improved thermal stability from dispersion of TiO_2 particles and the improved mechanical properties from dispersion of Al_2O_3 particles. Also, earlier research by the authors of this paper have shown that the co-electrodeposition of nickel with nanosized ceramic particles (such as Al_2O_3 or TiO_2) can improve oxidation resistance of pure forms of electrodeposited nickel but thus far, little research has been done on the effect of co-electrodeposition parameters, such as applied current density and concentration of the particles in the electrolyte solutions on oxidation behaviour of these coatings.

This paper focuses on the study of the performance of nickel-based cermet coatings when both Al_2O_3 and TiO_2 particles are incorporated in the nickel matrix under a variety of applied current densities (1, 2 and 3 A/dm^2) and then oxidized at 700 °C. Based on previous research on wear performance of the developed coatings, two group of electrolyte solution compositions (named A and B) were found to provide optimal mechanical properties [17] and therefore were selected for high temperature oxidation tests. In addition to each of these groups, two molar concentrations of particles (0.25 M and 0.5 M) in the electrolyte solution were produced and used for co-electrodeposition of coatings. For an analysis on high temperature oxidation performance of the selected coatings when co-electrodeposition parameters such as applied current density and concentration of the particles in the electrolyte solutions are alternated, specimens of coatings produced were co-electrodeposited on carbon steel substrate and then oxidized in dry air for 96 hours at 700 °C. The mass change per unit of area for each type of coating was measured at specific time intervals and then the method of least square and t-distribution was used for statistical analysis and obtaining confidence intervals of the results and also formulating the oxidation mass changes based on equation 8. Based on the results, the oxidation rate (k) and growth time (a) constants for each test condition were obtained. To evaluate coating performance at any given test conditions, the oxidation rate (k) and growth time (a) constants were analyzed and compared with each other. In addition SEM micrographs and EDS chemical analysis were used for further analysis of the coating performance and progression of the oxide layer. XRD analysis was also used for analysis of phase and compound formations as a result of oxidation reactions between the oxygen and constituents of the cermet coatings.

2 Experimental procedures

2.1 Materials

For this research two types of nanosized ceramic powders, alumina (α-Al_2O_3) and titania (TiO_2), were purchased from MK Impex Corp. Ltd. The purity for α-Al_2O_3 powder was 99.95% (with traces of Na: 300 ppm, Si: 3.5 ppm, Ca: 1.6 ppm, Fe: 0.2 ppm, and Co: 0.8 ppm). The purity for TiO_2 powder was 98% (with traces of Al: 20 ppm, Ca: 75 ppm, Mg: 65 ppm, Nb: 119 ppm, S: 165 ppm and Si: 102 ppm). The average grain size for Al_2O_3 powder was 20 nm and for the TiO_2 powder it was 50 nm (measured using TEM). The anode was made from a high purity (99.9%) nickel bar. The cathode (substrate) was made from a hot-rolled AISI-1018 carbon steel sheet and the specimens for co-electrodeposition were cut in a rectangular shape (length: 25 mm, width: 12.5 mm and thickness: 4 mm). The mill scale was removed by mechanical cleaning and the surface was prepared to a 600 grit finish. The specimens were then cleaned in alkaline solutions (E-Kleen 102-E™ and E-Kleen 129-L™) and finally an acid pickling solution (with 31% HCl) was used for removing any remaining grease or contaminates from the surfaces of the substrate specimens prior to the co-electrodeposition of the coatings.

2.2 Co-electrodeposition of cermet coatings

The chemical formula for Watt's bath was selected for the chemical composition of the electrolyte solution and the concentrations of Al_2O_3 and TiO_2 particles in the electrolyte solutions were obtained from previous research [2, 12, 17–18]. The electrolyte solutions were composed of two mixtures of Al_2O_3 and TiO_2 with two molar concentrations; A1 and B1 solutions have a particle molar concentration of 0.5 M, and A2 and B2 solutions have a particle molar concentration of 0.25 M. The pH of the electrolyte solutions was measured to be 4.0 to 4.2 and the temperature was kept between 50 °C to 55 °C. The coatings classification and the compositions of the electrolyte bath are summarized in Table 1. The coatings were produced using a direct current (DC) setup for electrodeposition. Current densities of 1, 2 and 3 A/dm^2 were applied with time as a variable to achieve a uniform coating thickness. Scanning electron microscopy (JEOL JXA-8200) was used to measure the average electrodeposited coating thickness. The produced average thickness was measured around 40 ± 5 μm. The particle contents (volume percent of for Al_2O_3 and TiO_2) in the nickel matrix of coatings were calculated using the "Image J" software program and are listed in Table 2.

2.3 Oxidation tests

Oxidation tests were conducted in an electric tube furnace (CARBOLITE-Eurotherm 2416CG) equipped with an automated temperature control system. The coated specimens were placed into a quartz tube and then heated up in the center of the furnace which was set at 700 °C. For each type of coatings, three specimens were co-electrodeposited and oxidized in the tube furnace for the given times. The weight of the specimens before and after oxidation tests were measured using an electric balance with an accuracy of 0.1 mg and the results were used for plotting mass change diagrams as a function of time. Two of these specimens were later cold mounted and used for metallographic SEM analysis. The remaining specimen was used for the XRD analysis. The oxidation test parameters are provided in Table 3.

Table 1: Type and concentration of electrolyte solutions and electrodeposition parameters

Coatings	Molar concentration	Weight of particles in electrolyte	Stirring speed	Electrolyte composition	Applied current density
A1	Al_2O_3: 0.25 M TiO_2: 0.25 M	Al_2O_3: 25.5 g/liter TiO_2: 20 g/liter	350 rpm	Standard Watt's bath solution: nickel sulphate hexahydrate (1 M), nickel chloride hexahydrate (0.2 M), and boric acid (0.5 M), dissolved in distilled water	Applied current density: 1, 2 and 3 [A/dm^2], time adjusted to achieve a thickness of 40 μm
B1	Al_2O_3: 0.375 M TiO_2: 0.125 M	Al_2O_3: 38.25 g/liter TiO_2: 10 g/liter	380 rpm		
A2	Al_2O_3: 0.125 M TiO_2: 0.125 M	Al_2O_3: 12.75 g/liter TiO_2: 10 g/liter	320 rpm		
B2	Al_2O_3: 0.1875 M TiO_2: 0.0625 M	Al_2O_3: 19.125 g/liter TiO_2: 5 g/liter	340 rpm		

Table 2: Particle counts (volume fractions) for co-electrodeposited coatings

Coating	Group	Applied current density		
		1 A/dm²	2 A/dm²	3 A/dm²
A	A1	(Al_2O_3: 4.9% ± 0.4%) (TiO_2: 5.0% ± 0.6%) Total: 9.9 vol.%	(Al_2O_3: 5.3% ± 0.5%) (TiO_2: 5.5% ± 0.4%) Total: 10.8 vol.%	(Al_2O_3: 5.8% ± 0.8%) (TiO_2: 6.0% ± 0.7%) Total: 11.8 vol.%
	A2	(Al_2O_3: 4.7% ± 0.3%) (TiO_2: 4.2% ± 0.3%) Total: 8.9 vol.%	Al_2O_3: 4.9% ± 0.4%) (TiO_2: 4.6% ± 0.5%) Total: 9.5 vol.%	Al_2O_3: 5.2% ± 0.7%) (TiO_2: 4.7% ± 0.1%) Total: 9.9 vol.%
B	B1	(Al_2O_3: 7.1% ± 0.5%) (TiO_2: 2.7% ± 0.3%) Total: 9.8 vol.%	(Al_2O_3: 6.8% ± 0.4%) (TiO_2: 2.4% ± 0.6%) Total: 9.2 vol.%	(Al_2O_3: 7.7% ± 0.7%) (TiO_2: 2.8% ± 0.7%) Total: 10.5 vol.%
	B2	(Al_2O_3: 6.3% ± 0.2%) (TiO_2: 2.2% ± 0.3%) Total: 8.5 vol.%	(Al_2O_3: 6.6% ± 0.2%) (TiO_2: 2.3% ± 0.2%) Total: 8.9 vol.%	(Al_2O_3: 6.9% ± 0.1%) (TiO_2: 2.4% ± 0.2%) Total: 9.3 vol.%

Table 3: High temperature oxidation tests parameters

Specimen	Temperature	Time	Specimen quantity
A1, B1, A2, B2	700 °C	6, 12, 24, 48, 72 and 96 hours	3 specimens for each type of coatings and time interval

2.4 Microstructural characterization

The grain size measurements of the powders was done by a Tecani F20-200 kV (the Netherlands) transmission electron microscope (TEM) in bright-field (BF) mode. The cross-sectional images of the oxidized specimens were taken using a JSM-8200 JEOL micro-probe (Tokyo, Japan) scanning electron microscopy (SEM) in the back-scattered electron mode (BSE). A Rigaku Multiflex X-ray diffactometer (Japan) was used for the X-ray diffraction spectroscopy (XRD) on the surfaces of the oxidized specimens.

2.5 Statistical analysis methods

Method of least square as described by ASTM G16 (Standard Guide for Applying Statistics to Analysis of Corrosion Data) was used for curve fitting on log-log plots. Both oxidation rate constant (k) and growth-rate time constant (a) were calculated and oxidation formulas based on the equation provided in Eq. (4) were written in a linear algebraic equation format ($y = mx + b$). Based on some preliminary pilot oxidation tests which were done during the early stages of this research, it was calculated that a sample population of 3 specimens when mass change is measured at least 6 times, can produce reliable results with a confidence limit over 90%. It was also calculated that this number of measurements could produce a sufficient amount of data for statistical analysis and measuring the mean and the standard deviation values. For all experiments, the confidence limit for each parameter was measured using the following formula:

$$\Delta = \pm \frac{t^* \times S}{\sqrt{n}} \tag{9}$$

where Δ is the limit that included the true mean value, t^* is the t-distribution, S is calculated standard deviation for each test and n is the sample population. The value for t^* (or t-distribution) can be calculated or obtained from statistical tables. Also for 3 specimens for each test parameter, the degree of freedom (DOF) is equal to 2 (DOF = $n - 1$ or $3 - 1 = 2$).

3 Results

3.1 Oxidation mass change results

The mass change per unit of area results for the coatings oxidized at 700 °C in dry air are illustrated in Figure 1. The corresponding logarithmic plots of the mass change results were calculated and presented in Figure 2. The individual measurements for each test condition are also

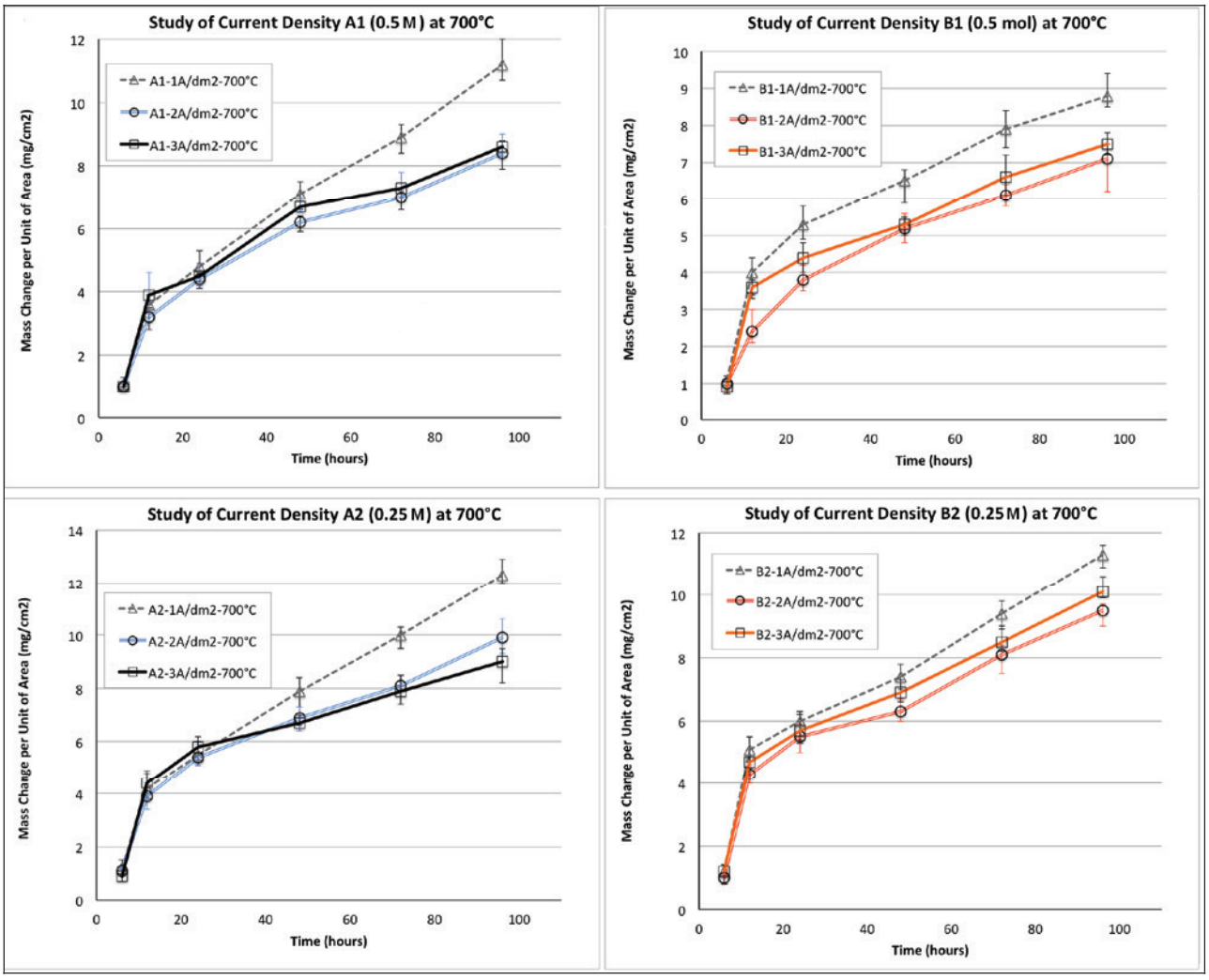

Fig. 1: Oxidation mass change as a function of time and applied current density for A1, B1, A2 and B2 at 700 °C

included on logarithmic graphs (Fig. 2) with respect to the calculated standard deviations and two confidence intervals of 68% (±1*S*) and 95% (±2*S*).

3.2 XRD analysis

Figure 3 represents the XRD analyses from the surfaces of two coatings (A1 and B1) for 96 hours at 700 °C. The matching angles for compounds for the coatings constituents were identified and shown on the graphs. The XRD analyses of the oxidized surfaces for both A1 and B1 did not find any significant compounds of aluminum on the oxidized surfaces. Meanwhile, the XRD results showed formation of Ni-Ti-O compounds ($NiTiO_3$ and Ni_3TiO_5) in the oxide layer of the coatings.

3.3 SEM images of the oxidized coatings

Figure 4 represents the BSE-SEM of the cross-sections of oxidized coating specimens co-electrodeposited with applied current densities of 1, 2 and 3 A/dm^2 and then oxidized for 96 hours at 700 °C in dry air.

4 Discussion

4.1 Particle content in nickel matrix

The amount of particle incorporation during the co-electrodeposition process is affected by many parameters such as particle geometrical characteristics, hydrody-

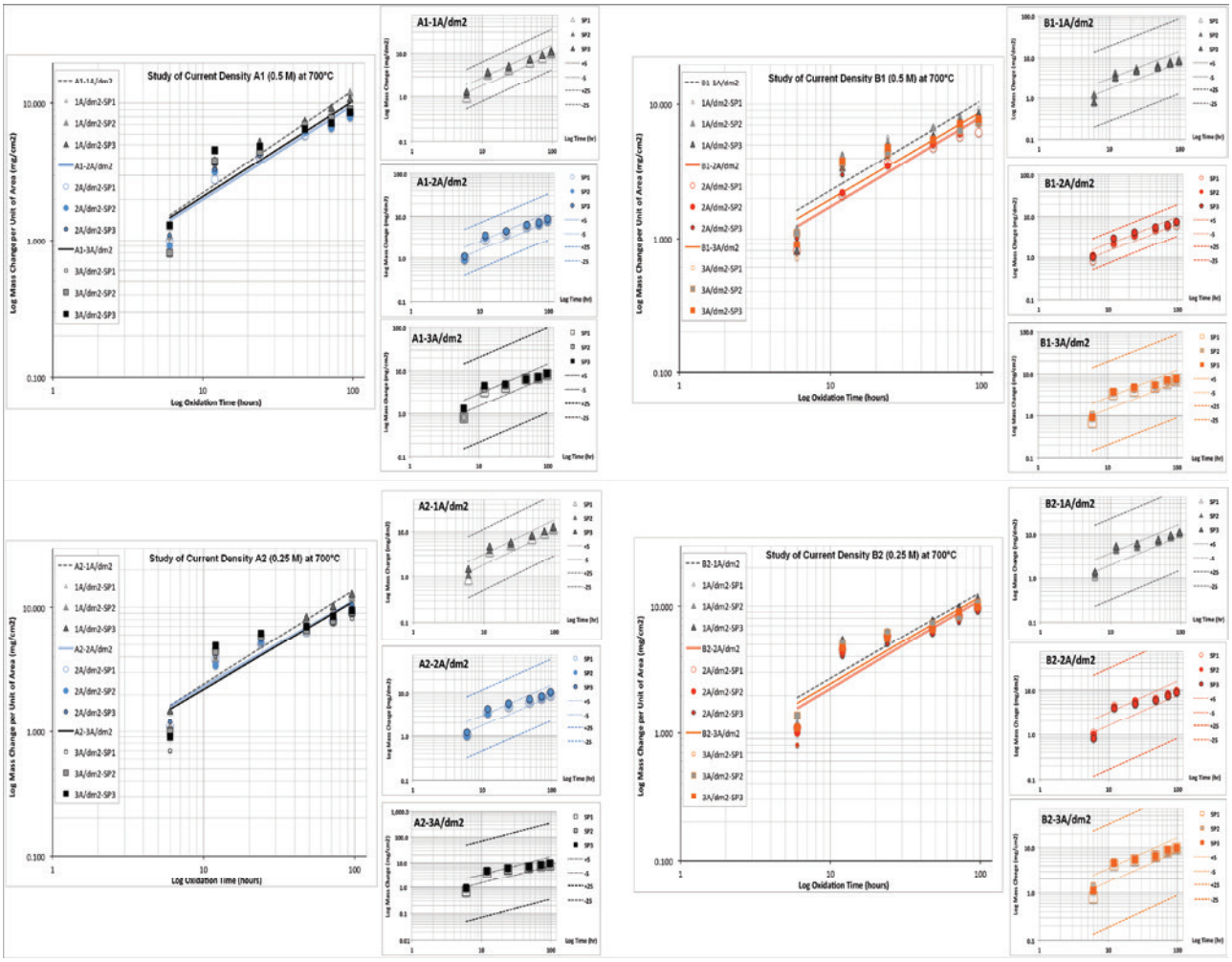

Fig. 2: Logarithmic plots (log-log plots) showing oxidation mass change as a function of time and applied current densities for cermet coatings oxidized at 700 °C: A1 (top-left), B1 (top-right), A2 (bottom-left) and B2 (bottom-right) – Standard deviations of individual measurements from log-log plots represent the variation from the mean value ±1*S* (68% confidence interval) and ±2*S* (95% confidence interval) are shown next to each plot

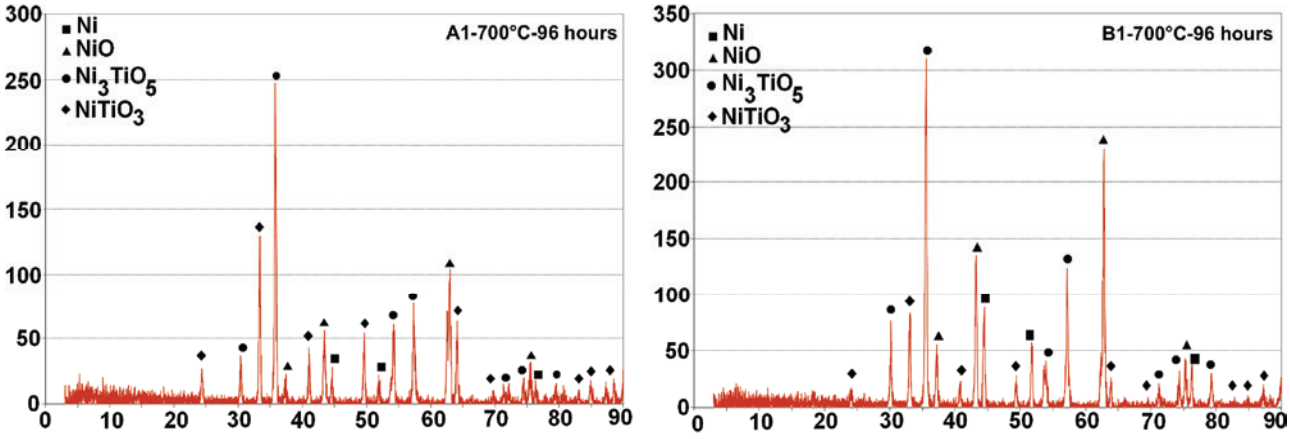

Fig. 3: XRD analyses for A1 and B1 coatings oxidized for 96 hours at 700 °C

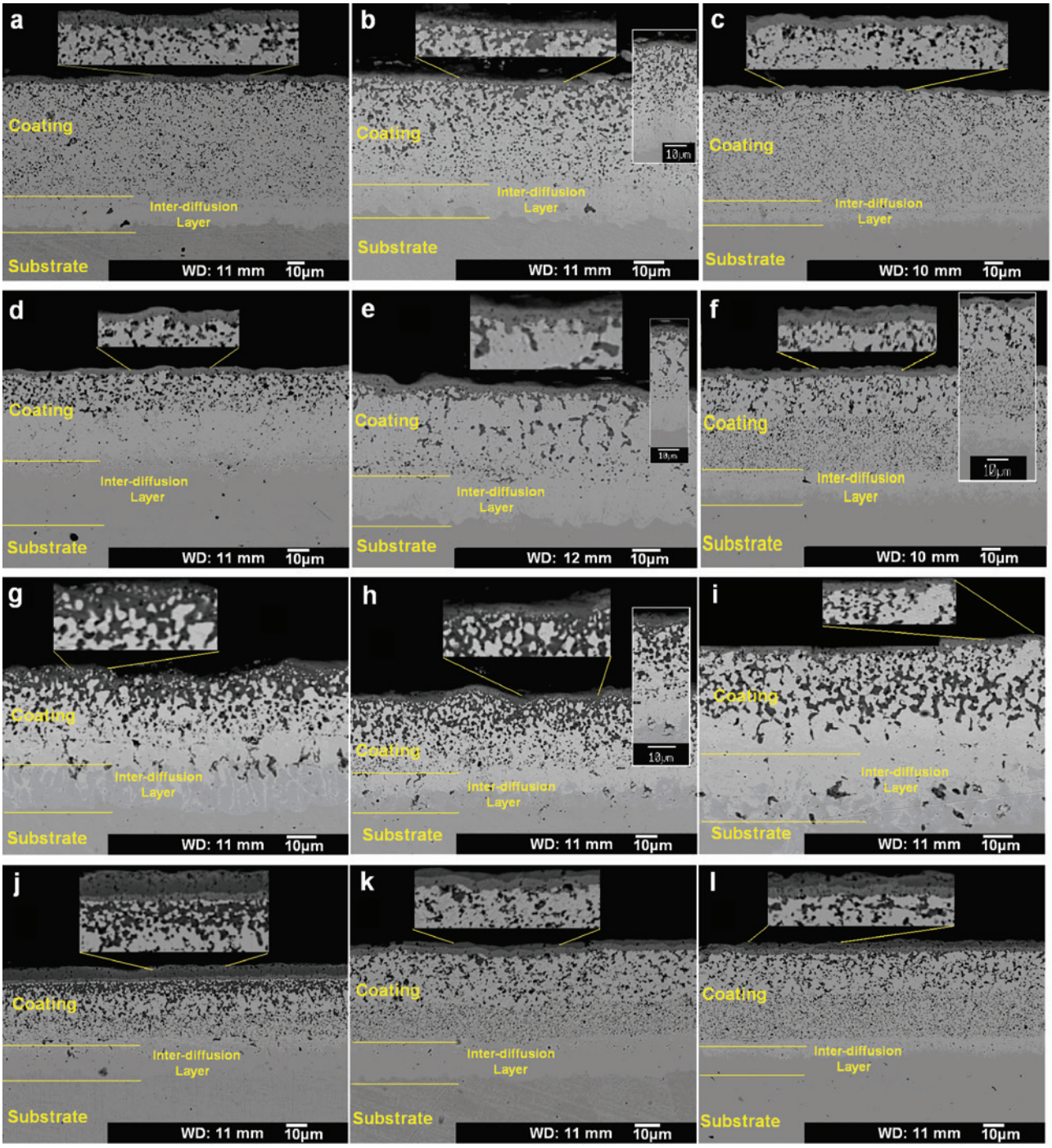

Fig. 4: SEM image of A1, B1, A2 and B2 oxidized at 700 °C for 96 hours. First row: A1 (0.5 M) co-electrodeposited by applied current densities of (a) 1 A/dm^2, (b) 2 A/dm^2, and (c) 3 A/dm^2. Second row: B1 (0.5 M); by current densities of (d) 1 A/dm^2, (e) 2 A/dm^2 and (f) 3 A/dm^2. Third row: A2 (0.25 M); by current densities of (g) 1 A/dm^2, (h) 2 A/dm^2, and (i) 3 A/dm^2. Fourth row: B2 (0.25 M); by current densities of (j) 1 A/dm^2, (k) 2 A/dm^2, and (l) 3 A/dm^2.

namics, and hydrokinetic. But most importantly it is affected by the concentration of particles in the electrolyte and also co-electrodeposition parameters such as applied current density [19]. In this research, the volume fraction measurements for Al_2O_3 and TiO_2 particles in the nickel matrix (see Table 2) showed that the volume fraction for each type of particle corresponded to its molar concentration in the electrolyte solution. The coatings produced

with type "A" electrolyte solutions (with an equal molar concentration of 0.25 M or 0.5 M for each type of particles) showed a relatively equal ratio for deposition of Al_2O_3 and TiO_2 particles in the nickel matrix. Similarly, the coatings produced with type "B" electrolyte solutions (with Al_2O_3 accounting for $\frac{3}{4}$ and TiO_2 accounting for $\frac{1}{4}$ of the total molar concentration) showed a proportional dispersion ratio for both Al_2O_3 and TiO_2 particles in the matrix that corresponded to their partial molar concentrations in the type "B" electrolyte solutions. A reduction in the amount of particles in the electrolyte solutions (i.e. from 0.5 mole to 0.25 mole) resulted in a lower number of particles deposited in the nickel matrix due to lower quantity of particles available at the deposition sites. It was also found that the alternation of current density from 1 to 3 A/dm^2 had an impact on the total volume fraction of particle incorporation in the nickel matrix for both types of coatings. In general by increasing the applied current density, the total particles incorporated in the nickel matrix was increased and this can be correlated to the increase in potential voltage between the cathode and anode through the electrolyte solutions. It should be noted that the DC setup for this study was a galvanostatic type in which the power supply provides a constant current to the circuit at the cost of a variable voltage (potential). The galvanostatic potential (E_g) for the electrodeposition circuit can be defined as:

$$E_g = i \times (R_e + R_c) \tag{10}$$

where i is the applied current, R_e is the ohmic resistance through the electrolyte, and R_c is the ohmic resistance through the anode-cathode electric circuit connection. It is acceptable to assume that for a constant increment of time, the total ohmic resistance for both electrolyte solutions and the associated cathode-anode circuit connection remains unchanged ($R_e + R_c = \text{constant}$), therefore by increasing the applied current i, the galvanostatic potential E_g (the electric field through the electrolyte) will also increase. An increase in galvanostatic potential as a result of increasing current density was observed during the electrodeposition process and measured to be between 2 to 3 volts. Therefore, it is expected that increasing the electric potential will cause an increase in the amount of attracting force on the particles ($F_E = E_g \times e$). Regardless of the mass, size and acceleration magnitude of the migrating particles, this increase in the electric force can result in a higher number of particles being dispersed into the nickel matrix. Also, by increasing the applied current density, both electrodeposition rates for nickel cations and electrophoresis attraction force on the ceramic particles will increase, there will be a competition between the rate of electrodeposition of nickel cations and the rate electrophoresis attraction of particles into the nickel matrix. By considering the parameters that can affect the electrodeposition rate of nickel cations ($W = Zit$) and comparing them with the parameters affecting zeta potential ($\zeta = 4\pi\eta\mu/DE$), it can be seen that a change in the amount of applied current density has a direct impact on the amount of nickel cation deposition. Meanwhile, this increase in the amount of applied current density has only an indirect impact on the zeta potential by causing a change in the field potential of the electrolyte. The mechanism for trapping ceramic particles in the metallic matrix during the co-electrodeposition of cermet coatings has not yet been fully understood, however, the force balance equations for electrophoresis deposition (see equations 3 to 6) suggest that a higher potential between the anode and cathode will increase the magnitude of excreted electric force on the ceramic particles ($F = E \times e$) resulting in higher zeta potentials. As a result of increasing the zeta potential, the dielectric pole potential on the surface of the ceramic particles will also increase, which in return, will increase the deposition rates of ceramic particles in the nickel matrix [2, 20]. Bund and Thieming et al. have investigated zeta potentials of Al_2O_3 and TiO_2 particles in nickel sulphate and nickel chloride electrolyte solutions [21–22]. Their result showed that in the presence of nickel salts (nickel sulphate, nickel chloride) in *Watt* type acidic electrolyte solutions (similar to the solutions used in this research), the electric charge on particles remains positive, which means a constant attraction towards the cathode. In addition, Kosmulski et al. and Erler et al. have investigated electrolyte solutions containing Al_2O_3 and TiO_2 particles with respect to the effects of changing the concentration of the electrolyte solutions on the zeta potential of nano-sized particles. They have found that the zeta potential sign (positive or negative charge) was unaffected by the change of the electrolyte concentration and similarly, the magnitude of zeta potentials were changed insignificantly (with high value of zeta potential around a pH of 4.0 in 1 M solutions) [23–24]. Therefore, it was concluded that changes in concentrations of Al_2O_3 and TiO_2 particles in the electrolyte solutions and also changes in applied current density have greater impact on the volume fraction of the dispersed particles in the nickel matrix as compared to changes in the amount of zeta potential of particles in the electrolyte solution.

4.2 Oxidation mass change of coatings – study of current density and electrolyte concentration

The effect of current density during co-electrodeposition on the oxidation mass change of the cermet coatings was statistically studied using the method of least square. The results are given in Figure 2. These graphs show that the oxidation rates were higher when the coatings were made by a current density of 1 A/dm^2 compared to coatings made by current densities of 2 A/dm^2 and 3 A/dm^2. The coatings made by current densities of 2 A/dm^2 and 3 A/dm^2 showed relatively close results for both A and B type coatings. In addition, the oxidation mass changes were greater when the coated specimens made from 0.25 M electrolyte solutions (A2 and B2) were compared to 0.5 M solutions (A1 and B1). The results for all coatings were plotted on logarithmic scales and their relevant oxidation rates (or k) and the growth-rate time constants (or a) for each current density were calculated and the results are listed in Tables 4 and 5. The mass change confidence limits for current density alternation experiments are also provided in Table 4. In addition confidence intervals of 68% (±1S) and 95% (±2S) were also plotted for each experiment (see Fig. 2) showing that the spread of measured data is close to mean value for all the coatings. The confidence limit values (ranges between 97.5% to 99.5%) showed reliable experimental results for the oxidation tests.

The higher oxidation mass change for solutions made with lower electrolyte concentrations (A2 and B2) com-

Table 4: Mass change confidence limits for oxidation tests

Coating	Current Density [A/dm^2]	Temp. [°C]	n	*Calculated "Δ"*	*Calculated "S"*	*Calculated "t"*	Confidence limit (C.L.)%
A1 (0.5 M)	1	700	3	0.8	0.097	14.285	C.L. > 99.5%
	2	700	3	0.5	0.107	8.094	99% < C.L. < 99.5%
	3	700	3	0.7	0.144	8.420	99% < C.L. < 99.5%
B1 (0.5 M)	1	700	3	0.6	0.138	7.531	99% < C.L. < 99.5%
	2	700	3	0.9	0.089	17.515	C.L. > 99.5%
	3	700	3	0.6	0.144	7.217	99% < C.L. < 99.5%
A2 (0.25 M)	1	700	3	0.6	0.119	8.733	99% < C.L. < 99.5%
	2	700	3	0.7	0.121	10.020	C.L. > 99.5%
	3	700	3	0.8	0.176	7.873	99% < C.L. < 99.5%
B2 (0.25 M)	1	700	3	0.7	0.139	8.723	99% < C.L. < 99.5%
	2	700	3	0.6	0.153	6.792	97.5% < C.L. < 99%
	2	700	3	0.5	0.153	5.660	97.5% < C.L. < 99%

Table 5: Oxidation rate and growth time constants – Function of current density and molar concentration of particles in electrolytes

Coating type		$m = a$	$b = \log(k)$	k	On logarithmic plot $y = mx + b$	$f(t) = \frac{\Delta m}{A} = kt^a$
A1	1 A/dm^2	0.74006	–0.38974	0.40762	y = 0.74006 × –0.38974	$f(t) = 0.40762 \times t^{0.74006}$
	2 A/dm^2	0.68466	–0.38342	0.41360	y = 0.68466 × –0.38342	$f(t) = 0.41360 \times t^{0.68466}$
	3 A/dm^2	0.69212	–0.36988	0.42670	y = 0.69212 × –0.36988	$f(t) = 0.42670 \times t^{0.69212}$
B1	1 A/dm^2	0.66679	–0.30655	0.49368	y = 0.66679 × –0.30655	$f(t) = 0.49368 \times t^{0.66679}$
	2 A/dm^2	0.67026	–0.43083	0.37083	y = 0.67026 × –0.43083	$f(t) = 0.37083 \times t^{0.67026}$
	3 A/dm^2	0.65274	–0.35942	0.43710	y = 0.65274 × –0.35942	$f(t) = 0.43710 \times t^{0.65274}$
A2	1 A/dm^2	0.75935	–0.37490	0.42179	y = 0.75935 × –0.37490	$f(t) = 0.42179 \times t^{0.75935}$
	2 A/dm^2	0.69227	–0.32716	0.47080	y = 0.69227 × –0.32716	$f(t) = 0.47080 \times t^{0.69227}$
	3 A/dm^2	0.70785	–0.36345	0.43306	y = 0.70785 × –0.36345	$f(t) = 0.43306 \times t^{0.70785}$
B2	1 A/dm^2	0.67321	–0.23890	0.57690	y = 0.67321 × –0.23890	$f(t) = 0.57690 \times t^{0.67321}$
	2 A/dm^2	0.69398	–0.33980	0.45730	$y = 0.69398 \times -0.33980$	$f(t) = 0.45730 \times t^{0.69398}$
	3 A/dm^2	0.67940	–0.28649	0.51702	$y = 0.67940 \times -0.28649$	$f(t) = 0.51702 \times t^{0.67940}$

pared to solution with higher concentration (A1 and B1) can be correlated to their lower volume fractions in the nickel matrix. Similarly, at lower applied current density, a smaller quantity of particles were incorporated in the nickel matrix (see Table 2) which can give a rise in higher oxidation rate for specimens co-electrodeposited with an applied current density of 1 A/dm^2. From Table 2, it is understood that increasing the applied current density from 1 A/dm^2 to 3 A/dm^2 increased the amount of volume fractions of particles deposited in the matrix. In general, the range for the increase in volume fraction of particles was between 1.0 to 1.9 vol.% for A1 and B1 coatings (from 0.5 M solutions) and it was between 0.7 to 0.8 vol.% for A2 and B2 coatings (from 0.25 M solutions). The results for oxidation mass changes (Fig. 1) and oxidation rate formulas (Table 5) also showed that A1 and B1 coatings (with greater quantities of dispersed particles in the matrix) have smaller mass change and oxidation rates compared to A2 and B2 coatings (with smaller quantities of dispersed particles in the matrix).

The increase in volume fraction of dispersed particles in the nickel matrix (particularly TiO_2) can influence the mass change rates with two possible mechanisms; firstly, a greater quantity of TiO_2 in the matrix can increase the quantity of formed Ni-Ti-O compounds such as $NiTiO_3$ on the surface and therefore, a reduction in the quantity of diffusing oxygen ions into the bulk of the coating can be expected. Secondly, the presence of a greater quantity of ceramic particles inside the nickel matrix reduces the quantity of nickel cations available to be oxidized during the oxidation process. However, it should be mentioned that the second mechanism cannot be directly interpreted as a result of a direct reduction in oxidation rate for the coating since there is less nickel to be oxidized in the first place.

4.2.1 Growth-rate time constants (*a*) and oxidation-rate constants (*k*)

Figure 5 provides a comparison between *a* and *k* constants for A1, B1, A2 and B2. Based on these graphs, alternation in current density has a relatively limited impact on growth-rate time constant (or *a*). Similarly the impact of current density on oxidation rate constant (or *k*) is more noticeable but remained low for all tested specimens.

The growth-rate time constants (or *a*) and oxidation-rate constants (or *k*) were found to be smaller in A1 and B1 coatings (with greater particle concentrations in electrolyte solutions and their dispersed volume fractions in the nickel matrix) compared to A2 and B2 coatings (with smaller particle concentrations in electrolyte solutions and their volume fractions in the nickel matrix). This difference in values for *a* and *k* can be correlated to the effect of dispersed particles in the nickel matrix (particularly TiO_2), on the diffusion rates of oxygen ions into the bulk of the nickel matrix. The XRD results (Fig. 3) have shown that Ni-Ti-O compounds (Ni_3TiO_5 and $NiTiO_3$) were thermodynamically formed and were present on the surface of oxidized coatings. Zeng et al. had shown that the formation of $NiTiO_3$ contributes to the lower oxidation rates for the alloys at temperatures lower than 750 °C [16]. The formation of Ni-Ti-O compounds in the oxide layer can have an impact on the oxidation rate of cermet coatings in two ways; firstly, some of the oxygen ions that are diffusing inward into the bulk of coating can react with nickel and be stored in the compound structures (Ni_3TiO_5 and $NiTiO_3$) resulting in a lower diffusion rate of oxygen and secondly, this reduction in the number of diffusing oxygen ions can cause a reduction in the rate of outward diffusion of nickel towards the forming oxide film.

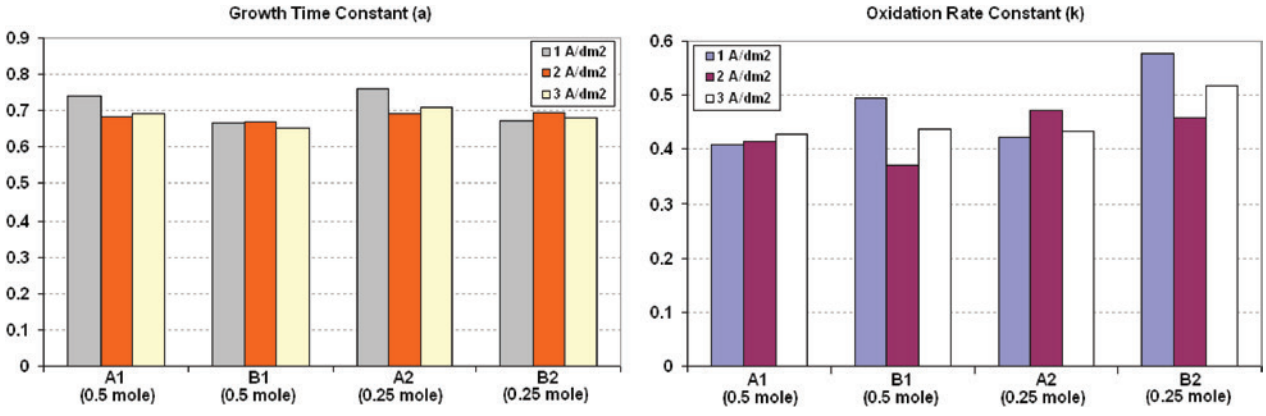

Fig. 5: Comparison between oxidation rate constant (*k*) and growth time constant (*a*) at 700 °C as a function of current density

4.3 Analysis of SEM images

Based on the images shown in Figure 4, the oxide layer on the surface was measured to be approximately 2 to 3 μm. The frequent dark spots that are visible within the bulk of the nickel matrix were also internal oxidation spots. The EDS analysis of these spots showed that they were rich in oxygen, nickel and iron (Fe) which suggested that some localized internal oxidation of iron cations from the substrate can have taken place in these spots which is a result of diffusion of iron cations from the steel substrate into these spots and then oxidized with excessive diffusing oxygen ions from the surface (oxide film/air interface). It should be noted that the difference in the amount of mass change per unit of area between the coatings made with similar molar concentrations (A1 to B1 or A2 to B2) is not remarkably different from each other, for instance, the mass change per unit of area difference between A1 and B1 coatings after 96 hours of oxidation at 700 °C (Fig. 1) is approximately 1 mg/cm^2 and this small difference can also occur under the influence of other factors such as localized internal oxidation of iron cations diffusing from the substrate into the nickel matrix.

4.4 Analysis of XRD results

The XRD results revealed that the dispersed TiO_2 particles in the nickel matrix formed at least two ternary Ni-Ti-O compounds (Ni_3TiO_5 and $NiTiO_3$). At 700 °C, both compounds were present in the oxidized surface of the coatings. The intermediate ternary compound between Ni, NiO and TiO_2 (anatase) is $NiTiO_3$ (nickel titanate) which forms in the presence of NiO and TiO_2 at around 600 °C [25–26]. $NiTiO_3$ is the only stable compound between Ni, NiO and TiO_2 that also can co-exist and form joined structures with TiO_2 particles [16, 27]. Both of these reactions can take place on the surface of the A1 and B1 coatings during the oxidation of nickel matrix and dispersed TiO_2 particles with oxygen from air. Ni_3TiO_5 was found in the XRD result which is a meta-stable phase formed at low temperatures (similar to the temperature used in this research) but only becomes a stable phase at much higher temperatures [28–29]. The formation of Ni-Ti-O compounds was correlated to the lower oxidation mass change for the coatings. Unlike TiO_2 particles, the XRD results did not find the formation of nickel aluminate ($NiAl_2O_4$) on the surface of the coatings. Based on the research conducted by Phillips et al. and Rhamdhani et al. [30, 31] the only intermediate ternary compound present in Ni, NiO, Al_2O_3 (corundum) phase diagram is $NiAl_2O_4$ (nickel aluminate) which can only form at temperatures above 650 °C [32]. The absence of nickel aluminate ($NiAl_2O_4$) on the surface could be caused by a relatively short oxidation time (maximum 100 hrs), which may not be long enough for a detectable quantity of nickel aluminate to form on the oxidizing surface of the coatings.

5 Conclusions

This paper investigates the high temperature oxidation behaviour of two groups of novel co-electrodeposited cermet coatings composed of both Al_2O_3 and TiO_2 nano-sized particles into a nickel matrix. Four types of coatings were produced based on two different compositions (the ratio between Al_2O_3 and TiO_2) and concentrations of particles (0.25 M and 0.5 M) in the electrolyte solutions. The results showed that the volume fraction for each type of dispersed particles (Al_2O_3 or TiO_2) in the nickel matrix corresponded proportionally to its partial molar concentration in the electrolyte solutions. To study the effects of applied current density (used in electrodeposition process) on oxidation behaviour of the coatings, three different current densities (1, 2 and 3 A/dm^2) were used. High temperature oxidation tests were conducted in dry air for 96 hours at 700 °C and the mass changed per unit of area at 6 specific time intervals for each sample were obtained. The method of Least Square line was used for curve fitting analysis and also calculating oxidation rate constants (k) and growth time constants (a). The statistical analysis showed a reliable statistical confidence level between 97.5% to 99.5% for the tests. The oxidation rate formulas were also calculated based on a method provided by other researchers, most notably Susan and Marder [10, 11]. The oxidation mass change measurements showed that an increase in the volume fraction of particles in the nickel matrix resulted in lower oxidation rates. Similarly an increase in applied current density from 1 to 2 and 3 A/dm^2 also reduced the oxidation rates for both A and B types of coatings. The XRD results showed formation of two Ni-Ti-O compounds (Ni_3TiO_5 and $NiTiO_3$) between the dispersed TiO_2 and nickel matrix. A reduction in oxidation mass change was recorded when the coatings were made by higher applied current density and this reduction in oxidation mass changes was correlated to the increase in volume fractions of dispersed particles in the matrix as a result of increasing the applied current density. The results for oxidation mass changes and oxidation rate formulas also showed that A1 and B1 coatings (with greater quantities of dispersed particles in the matrix) have smaller mass change and oxidation rates compared to A2 and B2 coatings (with smaller quantities of dispersed particles in the

matrix). The reduction in oxidation rates and mass change diagrams was correlated to two possible mechanisms that can take place simultaneously during the oxidation process. Firstly, the reduction in oxidation mass change was correlated to the formation of Ni-Ti-O compounds (i.e. Ni_3TiO_5 and $NiTiO_3$) in the oxide layer which can reduce the oxidation rate of cermet coatings by capturing some inward diffusing oxygen ions resulting in a lower number of nickel cations diffusing upward into the oxide layer. Secondly, it was explained that the presence of a greater quantity of ceramic particles inside the nickel matrix can indirectly reduce the quantity of nickel cations available to be oxidized with diffusing oxygen ions and as result, a lower oxidation mass change can be expected. However, it should be noted that the second mechanism shall not be directly interpreted as less oxidation rates for the cermet coatings.

The authors would like to thank the Department of Mechanical and Manufacturing Engineering, University of Calgary, Alberta, Canada and NSERC Canada, and Statoil Canada Ltd. for their financial support.

Received: September 4, 2013. Accepted: November 9, 2013.

References

[1] R. Gordon Moore, Catherine J. Laureshen, John D. M. Belgrave, Matthew G. Ursenbach, and S. A. (Raj) Mehta, Fuel 74, 1169–1175 (1995).
[2] D. R. Gabe, Principle of Metal Surface Treatment and Protection, Second Edition (Pergamon, 1978).
[3] Q. Feng, T. Li, H. Teng, X. Zhang, Y. Zhang, Ch. Liu, and J. Jin, Surface & Coating Technology 202, 4137–4144 (2008).
[4] L. M. Chang, J. H. Liu, and R. J. Zhang, Materials and Corrosion, No. 999 (Wiley-VCH Verlag, Weinheim, 2010).
[5] N. Birks, G. H. Meier, and F. S. Pettit, Introduction to the High-Temperature Oxidization, Second Edition (Cambridge University Press, 2006).
[6] J. R. Davis, Heat-Resistant Materials, p. 36 (ASM International Handbook, 1999).
[7] John M. West, Basic Corrosion and Oxidation, First Edition (Ellis Horwood Ltd., 1980).
[8] S. A. Bradford, Fundamental of Corrosion in Gases, Corrosion 13, 62–76 (ASM, 2001).
[9] M. A. Wahab, Solid State Physics – Structure and Properties of Materials, Chapter 6 (ASI Ltd., 2005).
[10] D. F. Susan and A. R. Marder, Oxidation of Metals 57, 131–158 (2002).
[11] D. F. Susan and A. R. Marder, Oxidation of Metals 57, 159–180 (2002).
[12] R. K. Saha, I. U. Haq, T. I. Khan, and L. B. Glenesk, Key Engineering Material 442, 187–194 (2010).
[13] P. Baghery, M. Farzam, A. B. Mousavi, and M. Hosseini, Surface & Coatings Technology 204, 3804–3810 (2010).
[14] L. Chen, L. Wang, Zh. Zeng, and J. Zhang, Material Science and Engineering A 434, 319–325 (2006).
[15] H. Gül, F. Kilic, S. Aslan, A. Alp, and H. Akbulut, Wear 267, 976–990 (2009).
[16] C. L. Zeng, M. C. Li, G. Q. Liu, and W. T. Wu, Oxidation of Metals 58, 171–184 (2002).
[17] M. A. Farrokhzad, G. C. Saha, and T. I. Khan, Surface and Coating Technology, in press (Available online 12 July 2013).
[18] M. A. Farrokhzad and T. I. Khan, Key Engineering Materials 510–511, 32–42 (2012).
[19] J. L. Stojak, J. Fransaer, and J. B. Talbot, Review of Electrocodeposition, Adv. Electrochem. Sci. Eng. (Wiley-VCH Verlag, Weinheim, 2002).
[20] J. O'M. Bockris and G. A. Razumney, Fundamental Aspects of Electrocrystallization (Plenum Press, New York, 1967).
[21] A. Bund and D. Thiemig, Surface & Coating Technology 201, 7092–7099 (2007).
[22] D. Thiemig and A. Bund, Surface & Coatings Technology 202, 2979–2984 (2008).
[23] M. Kosmulski et al., Colloids and Surface A: Physicochemical and Eng. Aspect. 301, 425–431 (2007).
[24] F. Erler, C. Jakob, H. Romanus, L. Spiess, B. Wielage, T. Lampke, and S. Steinhauser, Electrochimica Acta 48, 3063–3070 (2003).
[25] K. P. Lopes et al., Journal of Alloys and Compounds 468, 327–332 (2009).
[26] Qiu Ai-tao et al., Transactions of Nonferrous Metal Society of China, 21, 1808–1816 (Science Press & Elsevier, 2011).
[27] David Ortiz de Zarate et al., New Journal of Chemistry 29, 141–144 (2005).
[28] W. Laqua and H. Schmalzried, High Temperature Corrosion – NACE-6, 110–114 (National Association of Corrosion Engineers, 1982).
[29] D. J. Taylor, P. F. Fleig, S. T. Schwab, and R. A. Page, Surface and Coating Technology 465, 120–121 (1999).
[30] B. Phillips et al., Journal of The American Ceramic Society 46, 579–583 (ACS, 1963).
[31] M. A. Rhamdhani et al., Metallurgical and Materials Transactions B, 40B, 25–37 (2009).
[32] K. P. Trumble and M. Rühle, Acta Metallica Materialia 39, 1915–1924 (1991).